Optical and Quantum Electronics (2019) 51:225
https://doi.org/10.1007/s11082-019-1942-5

Diamagnetic susceptibility and optical properties of a spherical quantum dot: effects of the parabolic and the shifted parabolic potentials

Moletlanyi Tshipa[1]

Received: 11 March 2019 / Accepted: 15 June 2019 / Published online: 22 June 2019

Abstract
Centred charge donor related diamagnetic susceptibility and optical properties of a spherical *GaAs* quantum dot are presented. In particular, effects of intrinsic parabolic and shifted parabolic potentials on these quantities are investigated. This is theoretically achieved by solving the Schrödinger equation within the effective mass approximation. It is observed that the parabolic potential reduces the magnitude of the diamagnetic susceptibility while the shifted parabolic potential increases it. Other findings are that the parabolic potential blue-shifts both the absorption coefficient and the change in refractive index of quantum dots, while the shifted parabolic potential red-shifts these quantities. These features are discussed.

Keywords Diamagnetic susceptibility · Optical properties · Spherical quantum dots · Confining electric potential

1 Introduction

During these last decades, the study of impurity states in nanostructure semiconductors has become the subject of extensive investigation both theoretically and experimentally (Hsieh 2000; Ying et al. 1999). Due to their numerous applications in various disciplines such as nanoelectronics (Bhadra and Sarkar 2010), solar energy (Ataser et al. 2018), agriculture (Mandal and Ganguly 2011; Tekerek et al. 2011), optoelectronics (Kang et al. 2015; Rishinaramangalam et al. 2015; Ataser et al. 2018), thermoelectrics (Pennelli 2015; Cecchi et al. 2015), there is no doubt to the importance of quantum dots (QDs). This increasing interest in QDs has prompted many authors to intensify research on properties of QDs. QDs are very instrumental in realizing and manipulating qubits (Zhang et al. 2018). Qubits can be manipulated by application of electric and magnetic fields (Malkoc et al. 2016). Qubits can be stored in spins of charge carriers, but these are susceptible to leakage out of the computational space. Milivojević (2018) has suggested a way of minimising this leakage. It has also been reported

✉ Moletlanyi Tshipa
tshipam@mopipi.ub.bw

[1] University of Botswana, Private Bag 0022, Gaborone, Botswana

that QDs can be used to realise quantum gates that can, also, be manipulated by electric field, magnetic field and inter-QD distance (Burkard et al. 1999). The effects of cup-like and hill-like parabolic confining potentials on photoionization cross section (PCS) of a donor in spherical quantum dot (SQD) have been recently reported (Tshipa 2016). It was found that, as the cup-like parabolic potential intensifies, the peak of PCS becomes red-shifted for the $s \longrightarrow p$ transition and becomes blue-shifted for $p \longrightarrow d$, $d \longrightarrow f$ transitions, while the hill-like parabolic potential blue-shifted peak of PCS for $s \longrightarrow p$ transition and red-shifted the $p \longrightarrow d$ and $d \longrightarrow f$ transitions. Peter and Ebenezar (2009) have computed and compared the susceptibility of a hydrogenic donor in spherical confinement of harmonic oscillator-like and rectangular well-like potentials for a finite QD. Diamagnetic susceptibility of a confined donor in inhomogeneous quantum dots was recently reported by Rahmani et al. (2011).

In addition to diamagnetic susceptibility, optical properties of quantum structures have been studied as they yield insightful information on how to best utilize nanostructures for a wide range of optoelectronic and photonic applications (Chen et al. 2017). For example, it has been theoretically shown that it is possible to use quantum rings to detect terahertz radiation (Mobini and Solaimani 2018). Gul Kilic et al. (2018) studied optical properties of quantum dots with a centred impurity and found that transition energies depend strongly on the magnetic field, and the depth and range of impurity potential. The effect of Rashba spin-orbit interaction on absorption of a parabolic QD has also been investigated (Hosseinpour et al. 2016). It has also been shown that optical response of a quantum well can be modified by the Morse potential and tuned using electric field (Sakiroglu et al. 2017). Other investigations of optical properties were carried out in *GaAs* cone-like quantum dots (Gil-Corrales et al. 2017) and lens-shaped quantum structures (Zamani et al. 2017).

All of these motivated me to lead a new investigation on optical properties and diamagnetic susceptibility of a donor in a spherical QD using parabolic and shifted parabolic potentials, which are useful in controlling the electronic properties of nanostructures. To my knowledge, this result has not yet been reported in any literature.

This paper is organized as follows: Section 2 gives the details of theoretical framework, Sect. 3 presents the results and discussions. Concluding remarks are given in Sect. 4.

2 Theoretical framework

2.1 Wave functions and diamagnetic susceptibility

The envisaged system is a donor impurity located at the centre of a spherical quantum dot (SQD) of radius R. The intrinsic confining electric potentials of the SQD considered here vary parabolically with the radial distance from the centre of the SQD. The parabolic potential has a convex increase in the radial distance while the shifted parabolic potential has a convex decrease in the radial distance. Due to the spherical symmetry of the problem, the wave function is sought in the form $\Psi(r,\theta,\phi) = C_{lm}Y_{lm}(\theta,\phi)R(r)$, where C_{lm} is normalization constant, $Y_{lm}(\theta,\phi)$ are the spherical harmonics and $R(r)$ is the radial component of the wave function satisfying the Schrödinger equation

$$\frac{1}{r^2}\frac{d}{dr}\left(r^2\frac{d}{dr}R(r)\right) + \left\{\frac{2\mu}{\hbar^2}\left[E_{lm} + \frac{k_e e^2}{\epsilon_r r} - V(r)\right] - \frac{l(l+1)}{r^2}\right\}R(r) = 0 \tag{1}$$

with μ being the effective mass of the electron (of charge $-e$), $k_e = 1/(4\pi\epsilon_0)$ the Coulomb constant, where ϵ_0 is permittivity of free space and ϵ_r the relative dielectric constant of the SQD. The orbital momentum quantum number, $l(l = 0, 1, 2, ...)$, indicates the angular momentum of an electron whereas m is the magnetic quantum number. The spatially variant confining electric potential has been designated by $V(r)$ while E_{lm} are the electron's energy eigenvalues. The Schrödinger equation (Eq. 1) is solvable in terms of the Heun Biconfluent function (Ronveaux 1995; Hortaçsu 2013)

$$\begin{aligned} R(r) = A_{1lm} e^{g_1(r)} r^l HeunB(2l+1, \alpha, \beta, \gamma, g_2(r)) \\ + A_{2lm} e^{g_1(r)} r^{-(l+1)} HeunB(-(2l+1), \alpha, \beta, \gamma, g_2(r)) \end{aligned} \tag{2}$$

where $A_{1(2)lm}$ are constants, and coefficient A_{2lm} has to be taken as zero for the SQD due to the divergent nature of the second solution at the origin (centre).

The electric potential outside the quantum dot is considered to be infinitely high for electrons, while the potentials considered for the inside are the parabolic and the shifted parabolic.

Parabolic potential The SQD may be considered to have an intrinsic parabolic electric potential

$$V(r) = \frac{1}{2}\mu\omega_0^2 r^2 \quad \ldots (r < R)$$

and infinity elsewhere. Here, ω_0 is the angular frequency associated with the classical harmonic oscillator. The solution to the corresponding Schrödinger equation (Eq. 1) is expressible in terms of the Heun Biconfluent function (Eq. 2) with the parameters

$$\begin{aligned} \alpha &= 0 \\ \beta &= -\frac{2E_{lm}}{\hbar\omega_0} \\ \gamma &= \frac{4k_e e^2}{\hbar\epsilon_r}\sqrt{\frac{-\mu}{\hbar\omega_0}} \end{aligned} \tag{3}$$

and the arguments

$$g_1(r) = \frac{\mu\omega_0}{2\hbar} r^2 \tag{4}$$

and

$$g_2(r) = -i\sqrt{2g_1(r)}. \tag{5}$$

Requiring that the electron wave function should vanish at the walls of the SQD avails the energy spectrum of an electron in a SQD with a parabolic potential as

$$E_{lm} = -\frac{1}{2}\beta_R \hbar\omega_0, \tag{6}$$

with β_R satisfying the condition

$$HeunB(2l+1, \alpha, \beta_R, \gamma, g_1(R)) = 0. \tag{7}$$

Shifted parabolic potential This potential is maximum at the centre of the SQD and has a convex parabolic decrease in the radial distance to assume a minimum value (here taken as zero) at the radius;

$$V(r) = \frac{1}{2}\mu\omega_0^2(r-R)^2. \quad \ldots (r < R)$$

The solution to Eq. (1) for this potential is also in terms of the Heun Biconfluent function (Eq. (2)) but with the α parameter being non-zero;

$$\begin{aligned} \alpha &= 2\sqrt{\tfrac{\mu\omega_0 R^2}{-\hbar}} \\ g_1(r) &= \tfrac{\mu\omega_0}{2\hbar}(r-2R)r \\ g_2(r) &= -i\sqrt{\tfrac{\mu\omega_0}{\hbar}}r. \end{aligned} \tag{8}$$

β and γ are the same as those for the parabolic potential with the donor impurity. Application of the usual boundary conditions on the continuity of the wave function at the walls of the SQD as avails the energy spectrum as

$$E_{ml} = -\frac{\beta_R}{2}\hbar\omega_0, \tag{9}$$

where β_R is the value of β that satisfies the condition given in Eq. (7).

The wave functions are then used to evaluate the diamagnetic susceptibility of a donor impurity as (Mmadi et al. 2013; Jeice et al. 2016)

$$\chi_{dia} = -\chi_0\langle r^2\rangle/R^2 \tag{10}$$

where $\langle r^2\rangle$ is the quantum mechanical expectation value of the square of the radial distance from the centre of the SQD, evaluated by using the wave functions with the radial component (2) and $\chi_0 = (e^2R^2)/(6\mu\epsilon c^2)$, c being the speed of light.

2.2 Absorption coefficients and refractive index changes

The first order and third order contributions to absorption coefficient (AC) of a crystal can be evaluated via (Hosseinpour et al. 2016; Gil-Corrales et al. 2017; Zamani et al. 2017; Duque et al. 2016)

$$\alpha^{(1)}(\hbar\omega) = \frac{4\pi\alpha_{FS}\sigma_V}{n_r e^2}\hbar\omega|M_{fi}|^2\delta(\Delta E_{fi} - \hbar\omega), \tag{11}$$

$$\begin{aligned} \alpha^{(3)}(\hbar\omega, I_\omega) = -\frac{32\pi^2\alpha_{FS}^2\sigma_V I_\omega}{n_r^2 e^4\hbar\Gamma_{fi}}\hbar\omega|M_{fi}|^4 \\ \times\delta(\Delta E_{fi} - \hbar\omega)^2(1-\varpi_\alpha), \end{aligned} \tag{12}$$

where

$$\begin{aligned} \varpi_\alpha = \frac{|M_{ff} - M_{ii}|^2}{4|M_{fi}|^2} \\ \times\frac{(\hbar\omega - \Delta E_{fi})^2 - (\hbar\Gamma_{fi})^2 + 2\Delta E_{fi}(\Delta E_{fi} - \hbar\omega)}{(\Delta E_{fi})^2 + (\hbar\Gamma_{fi})^2}. \end{aligned} \tag{13}$$

In the above, α_{FS} is the fine structure constant, σ_V the electron volume density and n_r the refractive index of the crystal. M_{fi}, which are the dipole matrix elements coupling one state $|i\rangle$ to the other $|f\rangle$ are calculated according to

$$M_{pq} = e \int_V \Psi_p r \Psi_q dV$$

where $p, q = i$ or f and evaluated over the volume of the SQD V while $\hbar\Gamma_{fi}$ are the line widths associated with the different states indicated by the subscripts, considered in this communication to be $\hbar\Gamma_{fi} = 3.3$ meV. For computational purposes, the delta function has been replaced by the Lorentzian function

$$\delta(\Delta E_{fi} - \hbar\omega) \rightarrow \frac{\hbar\Gamma_{fi}}{\pi[(\Delta E_{fi} - \hbar\omega)^2 + (\hbar\Gamma_{fi})^2]}. \tag{14}$$

The summed absorption coefficient can then be written as

$$\alpha(\hbar\omega, I_\omega) = \alpha^{(1)}(\hbar\omega) + \alpha^{(3)}(\hbar\omega, I_\omega). \tag{15}$$

The corresponding first and third order contributions to the refractive index change are given by (Gul Kilic et al. 2018; Hosseinpour et al. 2016)

$$\frac{\Delta n^{(1)}}{(n_r)} = \frac{\sigma_V}{2\epsilon} |M_{fi}|^2 \frac{\Delta E_{fi} - \hbar\omega}{(\Delta E_{fi})^2 - (\hbar\Gamma_{fi})^2}, \tag{16}$$

and

$$\frac{\Delta n^{(3)}}{n_r} = -\frac{\mu_0 c I_\omega}{4\epsilon_0 n_r^3} \frac{\sigma_V |M_{fi}|^2}{[(\Delta E_{fi})^2 - (\hbar\Gamma_{fi})^2]^2} \varpi_n, \tag{17}$$

where

$$\begin{aligned} \varpi_n = {} & 4|M_{fi}|^2(\Delta E_{fi} - \hbar\omega) - |M_{ff} - M_{ii}|^2 \\ & \times \frac{\Delta E_{fi}(\Delta E_{fi} - \hbar\omega)^2 - (\hbar\Gamma_{fi})^2(3\Delta E_{fi} - 2\hbar\omega)}{(\Delta E_{fi})^2 + (\hbar\Gamma_{fi})^2}, \end{aligned} \tag{18}$$

μ_0 is the permeability of free space and $\epsilon = \epsilon_r \epsilon_0$. Similarly, the total change in refractive index (considered to third order) is

$$\frac{\Delta n}{n_r} = \frac{\Delta n^{(1)}}{n_r} + \frac{\Delta n^{(3)}}{n_r}. \tag{19}$$

3 Discussions

The effective mass used in these computations is $\mu = 0.067\,\mathrm{m_e}$, $\mathrm{m_e}$ being the free electronic mass, relevant to *GaAs* nanostructures. Figure 1 depicts the dependence of the scaled diamagnetic susceptibility on strengths of the parabolic (solid plots) and the shifted parabolic (dashed curves) potentials for the $l = 0$ state, in SQDs of radii $r_1 = R = 150\mathring{A}$,

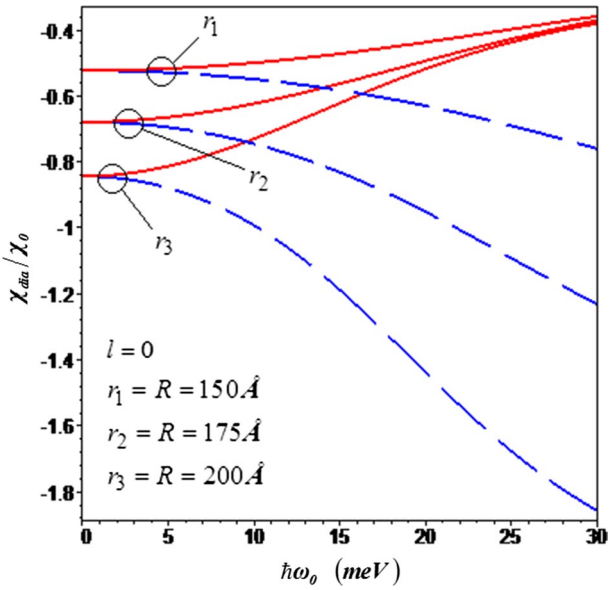

Fig. 1 The scaled diamagnetic susceptibility as a function of the potentials in SQDs of radii $r_1 = R = 150\text{Å}$, $r_2 = R = 175\text{Å}$ and $r_3 = R = 200\text{Å}$ for $l = 0$. The solid plots correspond to the parabolic potential while the dashed are associated with the shifted parabolic potential

$r_2 = R = 175\text{Å}$ and $r_3 = R = 200\text{Å}$. The scaling parameter χ_0 is of the order of $\sim 10^{-30}$ m^3. The parabolic potential reduces the magnitude of the diamagnetic susceptibility. This is due to the fact that the parabolic potential enhances localization around the centre of the SQD, which decreases $\langle r^2 \rangle$. Contrastingly, the nature of the shifted parabolic potential is such that it shifts electron wave functions towards the walls of the SQD. As such, the shifted parabolic potential increases the magnitude of the diamagnetic susceptibility. It can be noted from Fig. 1 that both potentials appreciably modify the diamagnetic susceptibilities of SQDs with larger radii than those of smaller radii. This is understandable from the fact that in a wider SQD, there is ample room for the parabolic (shifted parabolic) potential to constrict (dilate) wave functions.

Figure 2 shows the variation of the scaled diamagnetic susceptibility with radius of the SQD for the $l = 0$ and the $l = 1$ states. The solid curves marked η_1 correspond to an infinite spherical square quantum well (ISSQW) ($\hbar\omega_0 = 0$ meV), and those marked $\eta_2 (= \hbar\omega_0 = 15$ meV) are for parabolic potential (solid plots) and the shifted parabolic potential (dashed curves), each superimposed on an ISSQW, and each of strength $\hbar\omega_0 = 15$ meV. For an ISSQW, the magnitude of the diamagnetic susceptibility increases monotonically as a function of radius of the SQD. For an SQD with a parabolic potential, as radius of the SQD increases, the magnitude of diamagnetic susceptibility does not increase as much as for the ISSQW, due to the confinement from the parabolic potential. This is rather akin to the effect of the magnetic field on the diamagnetic susceptibility as the radius of the SQD is varied (Mmadi et al. 2013; Koksal et al. 2009). Contrastingly, the shifted parabolic potential enhances the magnitude of the diamagnetic susceptibility as a function of the radius of the SQD.

Figure 3 depicts absorption coefficient of an SQD of radius $R = 200\text{Å}$ as a function of energy of incident radiation of intensity $I_\omega = 95\,\text{MW/m}^2$, in the presence of the impurity. The centered donor impurity merely blue-shifts peaks of absorption coefficient. The plot marked η_1 corresponds to an ISSQW ($\hbar\omega_0 = 0$ meV), and the curve marked PP (SPP) corresponds to ISSQW with a superimposed parabolic potential (shifted

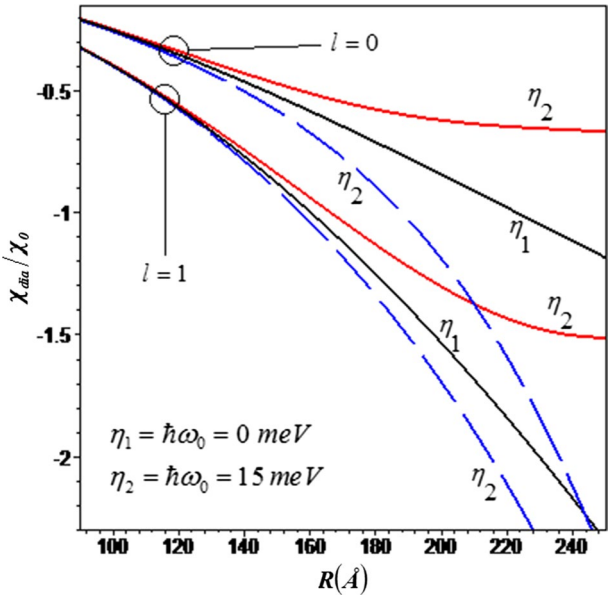

Fig. 2 The dependence of the scaled diamagnetic susceptibility on radius of the SQD for the ground state and the first excited state. The curves marked η_1 correspond to the infinite spherical square well (ISSQW) ($\hbar\omega_0 = 0$ meV), while those marked η_2 are associated with $\hbar\omega_0 = 15$ meV, solid for the parabolic potential, and dashed for the shifted parabolic potential

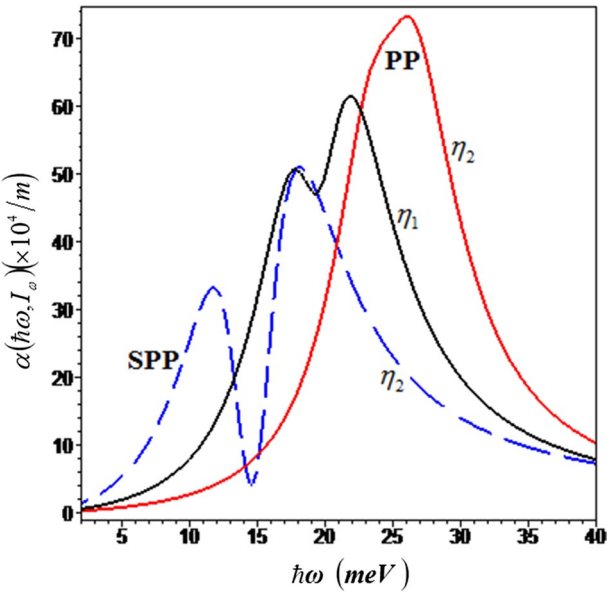

Fig. 3 The variation of absorption coefficient with radiation energy for an SQD of radius $R = 200\text{Å}$ in the presence of a donor impurity. The plot marked η_1 corresponds to an ISSQW ($\hbar\omega_0 = 0$) while the plot marked PP (SPP) corresponds to a SQD with an intrinsic parabolic potential (shifted parabolic potential), each of strength $\hbar\omega_0 = 15$ meV. The radiation intensity is $I_\omega = 95\,\text{MW/m}^2$

parabolic potential). On one hand, the parabolic potential affects the higher l states than it does the lower l states, therefore this potential increases transition energies. Transition energies are the differences in energies of states between which transitions occur. On the other hand, lower l states are more susceptible to the shifted parabolic potential, therefore this potential decreases transition energies. Consequently, the parabolic potential blue-shifts peaks of the AC while the shifted parabolic potential red-shifts the peaks. Another distinction between the effects of these two potentials on the AC is that

the parabolic potential enhances the magnitude of the AC, while the shifted parabolic potential decreases the magnitude of AC.

Figure 4 illustrates the dependence of AC of a SQD of radius $R = 200\mathring{A}$ on strengths of the parabolic electric confining potential (PP) and the shifted parabolic potential (SPP), for two values $\upsilon_1 = \hbar\omega = 18$ meV and $\upsilon_2 = \hbar\omega = 22$ meV of the photon energy. Intensity of the radiation field is $I_\omega = 95\,\mathrm{MW/m^2}$. The photon energy υ_1 is less than the energy differences between the ground state and the first excited state in an infinite spherical square quantum well (ISSQW) ($\hbar\omega_0 = 0$), while the photon energy υ_2 is slightly greater than the transition energy. In the case of υ_1, the shifted parabolic potential brings the system to resonance since it reduces transition energies. The parabolic potential, contrastingly, takes the system away from resonance since it increases transition energies. The situation is reversed for photon energy υ_2, which is more than the energy difference between the ground state and the first excited state in an ISSQW ($\hbar\omega_0 = 0$). In this case, it is the parabolic potential that brings the system to resonance, while the shifted parabolic potential drives the system away from resonance. Generally, the externally applied electromagnetic radiation reduces the AC considered up to third order.

Figure 5 depicts change in refractive index (CRI), $\Delta n_r/n_r$, as a function of photon energy for an SQD of radius $R = 200\mathring{A}$ in the presence of the donor impurity for $I_\omega = 150\,\mathrm{MW/m^2}$. The plots marked PP (SPP) are for an SQD with a parabolic potential (shifted parabolic potential) superimposed on an ISSQW. These are compared with the CRI for an ISSQW ($\hbar\omega_0 = 0$). For low radiation intensities ($I_\omega \approx 0$), the dependence of change in refractive index on photon energy is characterized by regions where $\Delta n_r/n_r$ increases with increasing photon energy, (called the normal dispersion region), and a region where it decreases with increasing photon energy (the anomalous dispersion region) (Farkoush et al. 2013). The point where the graph goes to zero in the anomalous dispersion region occurs when the photon energy matches transition energies. Since the parabolic potential enhances transition energies, this potential tends to blue-shift the graph of $\Delta n_r/n_r$ versus the photon energy. On the contrary, the shifted parabolic potential red-shifts the graph of

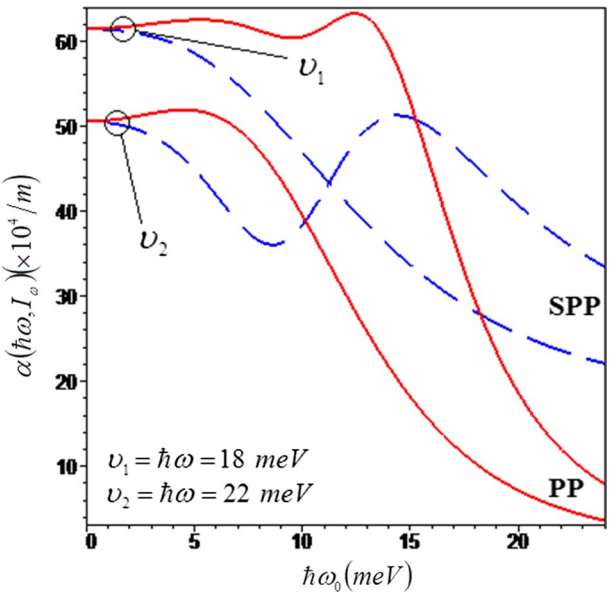

Fig. 4 The dependence of absorption coefficient of an SQD of radius $R = 200\mathring{A}$ on strengths of the parabolic and the shifted parabolic potentials for two photons energies, $\upsilon_1 = \hbar\omega = 18$ meV and $\upsilon_2 = \hbar\omega = 22$ meV. Intensity of the incident electromagnetic radiation is $I_\omega = 95\,\mathrm{MW/m^2}$

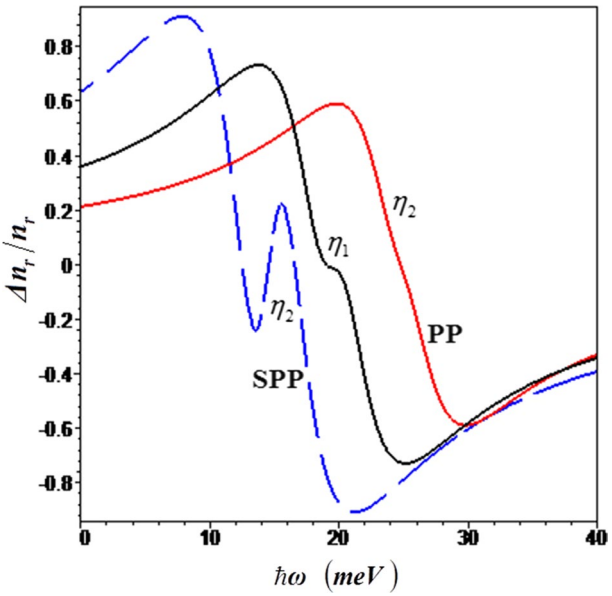

Fig. 5 The plot of the change in refractive index as a function of the photon for a spherical quantum dot of radius $R = 200\mathring{A}$ in the presence of a donor impurity, for $I_\omega = 150\,\mathrm{MW/m^2}$. The plot marked η_1 corresponds to the ISSQW $\hbar\omega_0 = 0$, the curve marked PP (SPP) is associated with the parabolic potential (shifted parabolic potential) superimposed in the ISSQW. The strength of the parabolic and the shifted parabolic potentials is $\hbar\omega_0 = 15\,\mathrm{meV}$

$\Delta n_r/n_r$ since it reduces transition energies. When CRI is considered up to third order, as intensity of the radiation field increases, the variation of the CRI with the photon energy ceases to possess one anomalous dispersion region, and develops a second one, nested between normal dispersion regions. However, the parabolic potential impedes the development of this second anomalous region, while the shifted parabolic potential promotes it. In fact, variation of the CRI with the photon energy has normal dispersion region sandwiched by anomalous dispersion regions as intensity of the radiation field increases further, characteristic of the third order CRI ($\Delta n^{(3)}/n_r$).

4 Conclusion

Donor related diamagnetic susceptibility of a spherical quantum dot and associated optical properties have been probed within the effective mass regime. In particular, the effects of the parabolic and the shifted parabolic potentials on these quantum quantities have been investigated. The results presented concur with interpretations of photoluminescence measurements performed on *GaAs* QDs (Birotheau et al. 1992; Höglund et al. 2009). These QDs were, of course, not spherical, partly due to the difficulty associated with nanofabricating spherical nanostructures. Lens-like nanostructures have proven to be easier to fabricate. Consequently, results obtained herein compared with those of lens-like structures would only differ slightly. For example, the parabolic and shifted parabolic potentials would have less effect on the diamagnetic susceptibility in the direction of greater spatial confinement than in the direction where the structure is wider. Secondly, transition energies for nanolenses are slightly higher than those for spherical structures, hence peaks of the AC and the anomalous dispersion region of the CRI in nanolenses would be slightly blueshifted (Zamani et al. 2017). The results of the present study, however, concur with theoretical investigations done on spherical QDs (Yakar et al. 2010; Keshavarz and Zamani 2013). It is observed that the parabolic potential has the proclivity to dwindle the magnitude of the

diamagnetic susceptibility, while the shifted parabolic potential increases it. The parabolic potential is also found to blue-shift both the absorption coefficient and the changes in the refractive index of a SQD, while the shifted parabolic potential redshifts the two quantities. This imbues nanotechnology with an additional avenue of modulating properties of nanostructures apart from tampering with the dimensions of the nanostructures. This can be advantageous in cases where the nanostructures are required to have specific dimensions and corresponding to specific values of, say, diamagnetic susceptibility and frequency of operation.

Acknowledgements The author would like to express gratitude to Tchakoua Theophile from National Radiation Agency of Cameroon, P. O. Box 33732, Yaounde, Cameroon, for the immense contributions he has made towards the development of this communication, and Z. Szabo, University of Botswana, for fruitful discussions and advice.

Compliance with ethical standards

Conflicts of interest The authors declare that they have no conflict of interest

References

Ataser, T., Sonmez, N.A., Ozen, Y., Ozdemir, V., Zeybek, O., Ozcelik, S.: Developing of dual junction gainp/gaas solar cell devices: effects of different metal contacts. Opt. Quantum Electron. **50**, 277 (2018)

Bhadra, J., Sarkar, D.: Field effect transistor fabricated from polyaniline-polyvinyl alcohol nanocomposite. Indian J. Phys. **84**(6), 693–697 (2010)

Birotheau, L., Izrael, A., Marzin, J.Y., Azoulay, R., Thiery-Mieg, V., Ladan, F.R.: Optical investigation of the onedimensional confinement effects in narrow gaas/gaalas quantum wires. Appl. Phys. Lett. **61**, 3023 (1992)

Burkard, G., Loss, D., DiVincenzo, D.P.: Coupled quantum dots as quantum gates. Phys. Rev. B **59**, 2070 (1999)

Cecchi, S., Llin, L.F., Etzelstorfer, T., Samarelli, A.: Review of thermoelectric characterization techniques suitable for sige multilayer structures. Eur. Phys. J. B **88**, 70 (2015)

Chen, R., Zheng, X., Jiang, T.: Broadband ultrafast nonlinear absorption and ultra-long exciton relaxation time of black phosphorus quantum dots. Opt. Express **25**(7), 7507–7519 (2017)

Duque, C.M., Acosta, R.E., Morales, A.L., Mora-Ramos, M.E., Restrepo, R.L., Ojeda, J.H., Kasapoglu, E., Duque, C.A.: Optical coefficients in a semiconductor quantum ring: electric field and donor impurity effects. Opt. Mater. **60**, 148–158 (2016)

Farkoush, B.A., Safarpour, G., Zamani, A.: Linear and nonlinear optical absorption coefficients and refractive index changes of a spherical quantum dot placed at the center of a cylindrical nano-wire: Effects of hydrostatic pressure and temperature. Superlattices Microstruct. **59**, 66–76 (2013)

Gil-Corrales, A., Morales, A.L., Restrepo, R.L., Mora-Ramos, M.E., Duque, C.A.: Donor-impurity-related optical response and electron raman scattering in gaas cone-like quantum dots. Physica B **507**, 76–83 (2017)

Gul Kilic, D., Sakiroglu, S., Sokmen, I.: Impurity-related optical properties of a laser-driven quantum dot. Physica E **102**, 50–57 (2018)

Höglund, L., Holtz, P.O., Petterson, H., Asplund, C., Wang, H., Malm, H., Almqvist, S.E., Petrini, E., Andersson, J.Y.: Optical pumping as artificial doping in quantum dots-in-a-well infrared photodetectors. Appl. Phys. Lett. **94**, 053503 (2009)

Hortaçsu, M.: Heun functions and their uses in physics. In Mathematical Physics: Proceedings of the 13th Regional Conference, Antalya, Turkey, October 27–31, 2010, pp. 23–39 (2013)

Hosseinpour, P., Soltani-Vala, A., Barvestani, J.: Effect of impurity on the absorption of a parabolic quantum dot with rashba spin-orbit interaction. Physica E **80**, 48–52 (2016)

Hsieh, C.-Y.: Lower lying states of hydrogenic impurity in a multi-layer quantum dot. Chin. J. Phys. **38**(3–I), 478–490 (2000)

Jeice, A.R., Jayam, S.G., Wilson, K.S.J.: Polaronic effects on diamagnetic susceptibility of a hydrogenic donor in nanostructures. Indian J. Phys. **90**(7), 805–809 (2016)
Kang, G., Yoo, J., Ahn, J., Kim, K.: Transparent dielectric nanostructures for efficient light management in optoelectronic applications. Nano Today **10**, 22–47 (2015)
Keshavarz, A., Zamani, N.: Optical properties of spherical quantum dot with position-dependent effective mass. Superlattices Microstruct. **58**, 191 (2013)
Koksal, M., Kilicarslan, E., Sari, H., Sokmen, I.: Magnetic-field effect on the diamagnetic susceptibility of hydrogenic impurities in quantum well-wires. Physica B **404**, 3850–3854 (2009)
Malkoc, O., Stano, P., Loss, D.: Optimal geometry of lateral gaas and si/sige quantum dots for electrical control of spin qubits. Phys. Rev. B **93**, 235413 (2016)
Mandal, G., Ganguly, T.: Applications of nanomaterials in the different fields of photosciences. Indian J. Phys. **85**(8), 1229–1245 (2011)
Milivojević, M.: Symmetric spin-orbit interaction in triple quantum dot and minimisation of spin-orbit leakage in cnot gate. J. Phys. Condens. Matter **30**, 085302 (2018)
Mmadi, A., Zorkani, I., Rahmani, K., Jorio, A.: Magnetic field effect on the diamagnetic susceptibility of hydrogenic donor in cylindrical quantum dot. Afr. Rev. Phys. **8**, 219–226 (2013)
Mobini, A., Solaimani, M.: A quantum rings based on multiple quantum wells for 1.2 to 2.8 thz detection. Physica E **101**, 162–166 (2018)
Pennelli, G.: Top-down fabrication of silicon nanowire devices for thermoelectric applications: properties and perspectives. Eur. Phys. J. B **88**, 121 (2015)
Peter, A.J., Ebenezar, J.: Diamagnetic susceptibility of a confined donor in a quantum dot with different confinements. J. Sci. Res. **1**(2), 200–208 (2009)
Rahmani, K., Zorkani, I., Jorio, A.: Diamagnetic susceptibility of a confined donor in inhomogeneous quantum dots. Phys. Scr. **83**, 035701 (2011). (1–6)
Rishinaramangalam, A.K., Ul Masabih, S.M., Fairchild, M.N., Wright, J.B., Shima, D.M., Balakrishnan, G., Brener, I., Brueck, S.R.J., Feezell, D.F.: Controlled growth of ordered iii-nitride core-shell nanostructure arrays for visible optoelectronic devices. J. Electron Mater. **44**(5), 1255–1262 (2015)
Ronveaux, A.: Heun's Differential Equations. Oxford University Press, Oxford (1995)
Sakiroglu, S., Kasapoglu, E., Restrepo, R.L., Duque, C.A., Sökmen, I.: Intense laser field-induced nonlinear optical properties of morse quantum well. Phys. Status Solidi **254**(4), 1600457 (2017)
Tekerek, S., Kudret, A., Alver, U.: Dye-sensitized solar cells fabricated with black raspberry, black carrot and rosella juice. Indian J. Phys. **85**(10), 1469–1476 (2011)
Tshipa, M.: The effects of cup-like and hill-like parabolic confining potentials on photoionization cross section of a donor in a spherical quantum dot. Eur. Phys. J. B. **89**, 177 (2016)
Yakar, Y., Çakir, B., Özmen, A.: Calculation of linear and nonlinear optical absorption coefficients of a spherical quantum dot with parabolic potential. Opt. Commun. **283**, 1795 (2010)
Ying, L., Hong-jing, X., Ben-kun, M., Jia-qiang, L., Jia-lin, Z.: Spectra of hydrogenic donor states in quantum-dot quantum well structures. Chin. Phys. Lett. **16**, 680–682 (1999)
Zamani, A., Azargoshasb, T., Niknam, E., Mohammadhosseini, E.: Absorption coefficient and refractive index changes of a lens-shaped quantum dot: Rashba and dresselhaus spin-orbit interactions under external fields. Optik **142**, 273–281 (2017)
Zhang, X., Li, H.-Q., Wang, K., Cao, G., Xiao, M., Guo, G.-P.: Qubits based on semiconductor quantum dots. Chin. Phys. B **27**(2), 020305 (2018)